

Achieving centimetre-scale supercollimation in a large-area two-dimensional photonic crystal

PETER T. RAKICH*[†], MARCUS S. DAHLEM*, SHEILA TANDON, MIHAI IBANESCU, MARIN SOLJAČIĆ, GALE S. PETRICH, JOHN D. JOANNOPOULOS, LESLIE A. KOLODZIEJSKI AND ERICH P. IPPEN

Center for Material Science and Engineering, and Research Laboratory of Electronics, Massachusetts Institute of Technology, Cambridge, Massachusetts 02139, USA

*These authors contributed equally to this work

[†]e-mail: rakich@mit.edu

Published online: 15 January 2006; doi:10.1038/nmat1568

Diffraction, a fundamental process in wave physics, leads to spreading of the optical beams as they propagate. However, new photonic crystal (PhC) meta-materials can be nano-engineered to generate extreme anisotropy, resulting in apparent propagation of light without diffraction. This surprising phenomenon, called supercollimation, effectively freezes the spatial width of a light beam inside a PhC, observed over a few isotropic diffraction-lengths^{1–6}. However, using such experiments to predict the behaviour for longer propagation lengths is difficult, as a tiny error in a measured width can extrapolate to order unity uncertainty in the width at distances over hundreds of diffraction-lengths. Here, supercollimation is demonstrated in a macroscopic PhC system over centimetre-scale distances, retaining spatial width confinement without the need for waveguides or nonlinearities. Through quantitative studies of the beam evolution in a two-dimensional PhC, we find that supercollimation possesses unexpected but inherent robustness with respect to short-scale disorder such as fabrication roughness, enabling supercollimation over 600 isotropic diffraction-lengths. The effects of disorder are identified through experiments and understood through rigorous simulations. In addition, a supercollimation steering capability is proposed.

A natural metric for the scale of collimation experiments is the length over which a gaussian optical beam would normally spread by a factor of $\sqrt{2}$ in an isotropic medium, referred to as the isotropic diffraction-length. It is defined as $L_d = \pi \cdot w^2 / \lambda_x$ where w is the gaussian beam waist radius, $\lambda_x = 2\pi/k_x$ is the wavelength of light in the direction of propagation and k_x its wavevector. The utility of supercollimation is strongly linked to the distance over which it can be maintained or, more accurately, the number of diffraction-lengths possible. This figure of merit is important as it dictates the maximum density and complexity of optical circuits on the basis of supercollimation^{4–9}. Experimental studies of supercollimation have used mesoscopic ($\sim 100 \mu\text{m}$) systems to estimate the beam evolution in PhCs. Estimates of

this type translate to large uncertainties in macroscale properties of these meta-materials, which are critical for applications such as optical interconnects and non-diffractive imaging. To address this issue, we present a quantitative study of supercollimation, using both near-field scanning optical microscopy (NSOM) and confocal imaging techniques, and we demonstrate that this phenomenon is indeed possible over as much as 600 isotropic diffraction-lengths. This represents an improvement of two orders of magnitude over previous demonstrations, and is an important enabling step towards the creation of high-density and low-cost optical interconnects⁹.

The physical system under study consists of a centimetre-scale two-dimensional PhC slab formed by a square lattice of air holes in a 205-nm-thick silicon film. Vertical confinement of the light in the film is achieved through index guidance, with an air over-cladding and a 3.0- μm -thick SiO_2 under-cladding. A scanning electron micrograph of the large-area PhC possessing about 10^9 lattice points, fabricated through interferometric lithography¹⁰, is shown in Fig. 1a (micrographs obtained with an LEO SEM system). The lattice constant ($a = 350 \text{ nm}$) and hole radius ($r = 0.3a$) were chosen to produce an ultraflat dispersion surface in the 1.5 μm wavelength range for transverse electric (TE)-polarized light (electric field parallel to the two-dimensional plane). The projected band structure of the PhC slab under study was computed with a three-dimensional frequency-domain eigenmode solver¹¹. The indices of refraction used for the simulations were $n_{\text{silicon}} = 3.5$ and $n_{\text{silica}} = 1.45$. Figure 1b shows several equifrequency contours for the lowest band of the PhC, with magnified views of the relevant contours near the wavelengths of interest (Fig. 1c). For the normalized frequency $\omega = a/\lambda = 0.228$, the PhC shows remarkably little spatial dispersion in a transverse wavevector (k_y) range from -0.05 to 0.05 ($2\pi/a$).

For comparison with experiments, the beam evolution was simulated through the beam propagation method (BPM) based on the computed dispersion surfaces (Fig. 2a–c). As expected, the beam divergence is negligible for $\omega = 0.228$. It is interesting

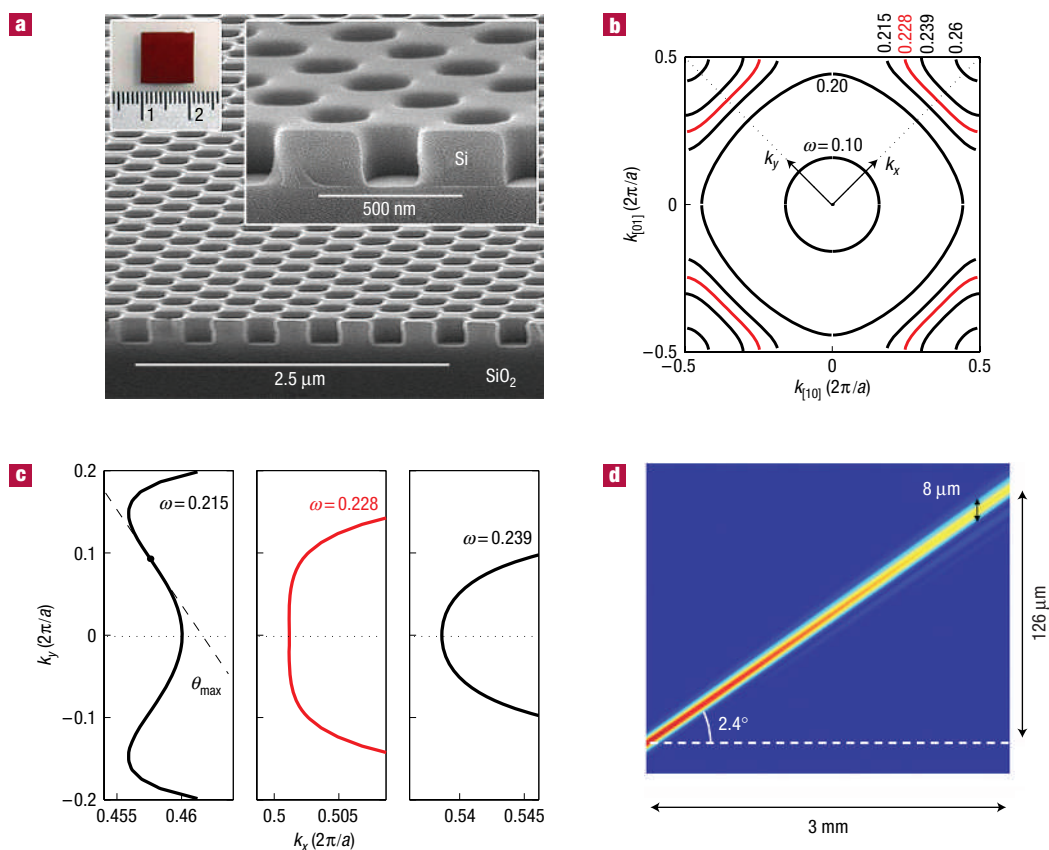


Figure 1 Physical system under study. **a**, SEM image of PhC over a large area. Left inset: Digital photo of the full 1 cm × 1 cm sample. Right inset: High-magnification SEM image of the PhC structure. **b**, Equipfrequency contours for the lowest band of the fabricated PhC. **c**, Magnified (and 45°-rotated) view showing the ‘flat’ region of contours from **b**. **d**, BPM simulation of supercollimation at the inflection point.

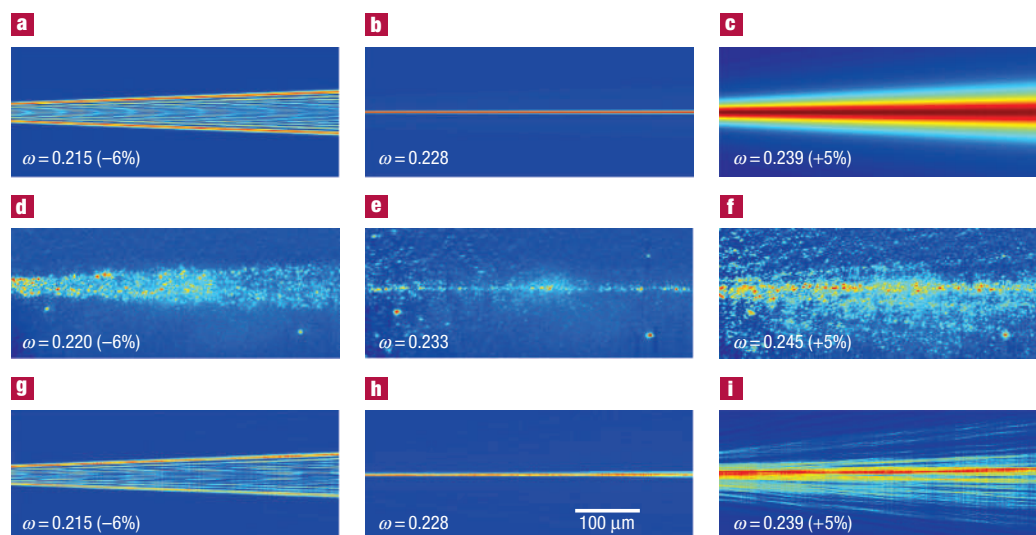


Figure 2 Experimental and theoretical evolution of the beam in the PhC. **a–c**, Theoretical beam evolution generated through BPM for $\omega = 0.215$, 0.228 and 0.239 , to be compared with experiment (**d–f**). **d–f**, Top-view experimental images of light travelling through the PhC for $\omega = 0.220$, 0.233 and 0.245 (1,590, 1,500 and 1,430 nm) obtained through light scattered from the beam with an infrared camera. Each image is approximately 500 μm to the right of the point of excitation. **g–i**, BPM simulations of the beam evolution (for $\omega = 0.215$, 0.228 and 0.239) including the effects of disorder. The inclusion of disorder in the simulation primarily modifies the beam evolution at high frequencies, resulting in beam break-up (similar to that observed in **f**). Simulations used an r.m.s. hole-radius variation of 0.6 nm. The BPM model used to generate **a–c** and **g–i** is based on computed dispersion surfaces similar to those shown in Fig. 1c. The supercollimation effect is observed around 1,500 nm and beam-spreading appears for wavelengths above and below this value.

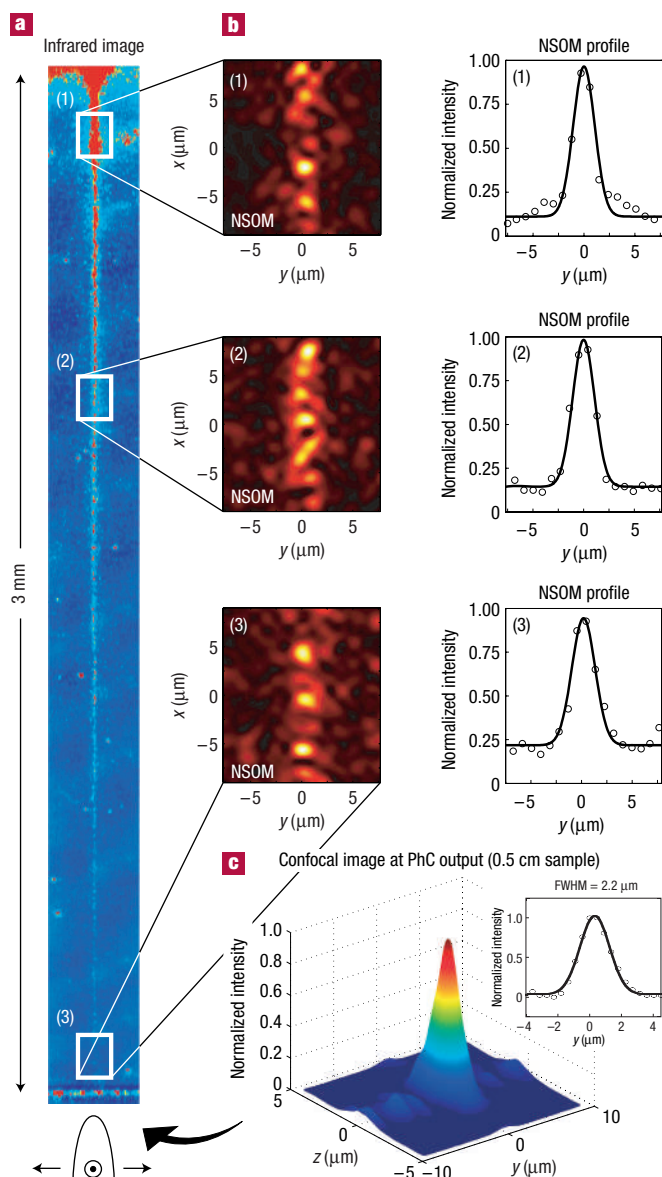


Figure 3 Supercollimation over a 0.3 cm sample. **a**, Top view of the TE light guided along the PhC, acquired with an infrared camera. **b**, NSOM images of the collimated beam at positions labelled (1)–(3) in **a** (corresponding to 0.02, 0.10 and 0.30 cm along the device). Next to each NSOM image is a beam cross-section obtained from the intensity map (with a gaussian fit). **c**, Confocal image (shown as a surface plot) at the output of an identical 0.5-cm-long PhC, showing the TE-beam profile at the supercollimation wavelength. Right inset: Line-scan of the beam profile (circles) and a gaussian fit (solid line), showing a FWHM of 2.2 μm.

to note that at frequencies below the supercollimation frequency ($\omega = 0.215$), the dispersion surface $k_x(k_y)$ has two inflection points. This results in a sharp edge of the beam profile whose divergence angle is determined by the angles ($\pm\theta_{\max}$) at the inflection point¹². In contrast, the edge of the beam is rather poorly defined in Fig. 2c, where the dispersion surface is more reminiscent of the isotropic case.

Evolution of the beam in the PhC is visualized experimentally by collecting light scattered through nanoscale roughness. Excitation of a TE-polarized propagating beam was achieved using

a tunable laser source and a high-numerical-aperture lensed fibre, producing an initial beam full-width at half-maximum (FWHM) of 1.0 μm at the PhC input. The scattered light from the PhC was imaged with a Hamamatsu (C5332) infrared camera (Fig. 2d–f) for normalized frequencies of 0.220, 0.233 and 0.245 (or wavelengths of 1,590, 1,500 and 1,430 nm, respectively). Each image is shown over a 500 μm × 225 μm area located approximately 500 μm to the right of the input. It should be noted that simulations predict a supercollimation wavelength of 1,535 nm, whereas the fabricated system shows supercollimation at 1,500 nm. This corresponds to a 2% discrepancy, well within the experimental uncertainty. For comparison with experiments, the simulations are shown with comparable frequency shifts about the supercollimation frequency. Although the rapid oscillations expected in the transverse beam profile of Fig. 2d are not resolvable by this imaging mechanism, the divergence angles of the experimental images (Fig. 2d–f) agree reasonably well with the simulated beams (Fig. 2a–c).

Nevertheless, a close inspection of Fig. 2f reveals beam break-up not captured in the theoretical model of a perfect PhC. This is because the theoretical model does not include disorder, resulting from variations in the etch process. Such roughness, although small and largely uncorrelated, is non-negligible (r.m.s. fluctuation in the hole radius of 0.6 nm). Interference lithography produces a very uniform average hole radius and lattice constant across the entire sample. Therefore, the following correction to the physical model is justified: light propagates in a material whose dispersion relation is determined by the perfect PhC, and this material has small local (random phase) perturbations centred at the positions of the holes of the underlying PhC lattice. This model of disorder is easily incorporated into BPM simulations by distributing random phase changes at the lattice points with a phase amplitude estimated from the r.m.s. fluctuation in hole radius. Such simulations are shown in Fig. 2g–i. These simulations reproduce the qualitative features of the experimental plots, thus confirming that the disorder present in the system is indeed responsible for the beam break-up. Furthermore, the angular separation among the broken beams can be estimated using properties of discrete Fourier transforms, the knowledge of the dispersion relation, the size of the input beam and the lattice spacing. Estimates of this type lead to angular separations of about 3°–6°, which are consistent with experimental observations.

The physical limitations of these PhC meta-materials can be explored further at centimetre scales. An image of scattered light (similar to those in Fig. 2d–f) is shown in Fig. 3a, over a 0.3-cm-long sample. Supercollimation is apparent over the entire length without any resolvable beam divergence, for $\lambda = 1,500$ nm. To further quantify the spatial evolution of the beam, coarse contact-mode NSOM was applied at various positions along the sample, detecting light scattered from the evanescent field of the PhC by a tapered glass-fibre probe¹³. Three images taken by this method (at positions 0.02, 0.10 and 0.30 cm from the input) are shown in Fig. 3b. Careful analysis reveals near-gaussian beam shapes and FWHM beam widths of 2.5, 2.5 and 2.7 μm (± 0.2 μm). Deconvolution with the imaging impulse response is necessary to estimate the beam width, yielding values of 2.1, 2.1 and 2.3 μm (± 0.2 μm), respectively. This demonstrates a remarkably stationary beam width over the entire 0.3 cm device.

It is important to note that although the beam width used to excite the PhC is 1.0 μm FWHM, the collimated beam observed along the PhC has an approximately unchanging width of 2.0 μm FWHM. Careful simulations of the beam evolution inside the PhC reveal that, over the first propagation distance of approximately 100 μm, the 1.0 μm input beam sheds some of its transverse wavevector components through diffraction and evolves into a supercollimated beam of 2.0 μm FWHM. The BPM simulations

indicate that a 2.0 μm beam is the smallest supercollimated beam that the fabricated PhC can support over centimetre lengths, and experimental observations are consistent with these findings.

Propagation losses of (3.6 ± 0.5) dB mm^{-1} were measured from the scattered light images (obtained with InGaAs camera SU320-1.7RT). This attenuation made NSOM measurements difficult for device lengths greater than 0.3 cm. However, a collimated beam could still be observed by imaging the mode exiting the PhC with a confocal scanning microscope. Figure 3c shows a confocal image of the TE light collected at the end of a 0.5 cm PhC device at the supercollimation wavelength ($\lambda = 1,495$ nm). A gaussian fit and deconvolution with the imaging impulse response reveal a beam FWHM of 2.0 ± 0.2 μm , clearly demonstrating negligible spreading of the beam over the entire PhC length. As the isotropic diffraction-length for this PhC is 13.2 μm , these observations are consistent with supercollimation over about 380 isotropic diffraction-lengths. Similar studies at numerous positions along the entire PhC, and in the different symmetry directions, revealed virtually identical optical properties over the entire area of the PhC. Further studies of a 0.8 cm PhC device yielded measurements of beams with similar transverse profiles and a figure of merit closer to 600 isotropic diffraction-lengths.

Finally, it is interesting to note that one can use the inflection points to perform wavelength-dependent supercollimation beam-steering. Figure 1d illustrates supercollimation for a case in which the excitation wavevector spectrum is centred at an inflection point ($k_y = 0.093(2\pi/a)$ in Fig. 1c). The input beam is 6 μm wide and $\omega = 0.215$, 6% below that used for supercollimation at $k_y = 0$. At the end of 0.3 cm of propagation, the beam has widened to 8 μm and has shifted by 126 μm in the transverse direction (2.4°) from the axis of straight (0°) propagation. If ω approaches 0.228 and k_y is kept at an inflection point, the beam will steer to the 0° propagation direction. This angle-dependent supercollimation effect can be used for frequency-dependent beam-steering over the large 6% frequency bandwidth. Even though the topology of the dispersion contour at the inflection points is quite different from the case at $\omega = 0.228$ (in Fig. 1c), supercollimation is still possible over more than 10 diffraction-lengths. Such steering mechanisms could prove useful in interconnection architectures for coarse wavelength selective routing⁹.

The established macroscopic nature of supercollimation demonstrates that control of the PhC structure at nanoscales enables the realization of an effective bulk medium with anomalous photonic properties on the macroscopic scale. In addition, the $\omega(k)$ design possibilities and the intrinsic lack of coupling alignment and cross-talk between intersecting supercollimated beams opens windows of opportunity for new beam-steering mechanisms, non-diffractive imaging and on-chip optical interconnects, over macroscopic length scales.

Received 1 August 2005; accepted 14 November 2005; published 15 January 2006.

References

1. Kosaka, H. *et al.* Self-collimating phenomena in photonic crystals. *Appl. Phys. Lett.* **74**, 1212–1214 (1999).
2. Kosaka, H., Kawashima, T., Tomita, A., Sato, T. & Kawakami, S. Photonic-crystal spot-size converter. *Appl. Phys. Lett.* **76**, 268–270 (2000).
3. Wu, L. J., Mazilu, M. & Krauss, T. F. Beam steering in planar-photonic crystals: From superprism to supercollimator. *J. Lightwave Technol.* **21**, 561–566 (2003).
4. Prather, D. W. *et al.* Dispersion-based optical routing in photonic crystals. *Opt. Lett.* **29**, 50–52 (2004).
5. Pustai, D. M., Shi, S. Y., Chen, C. H., Sharkawy, A. & Prather, D. W. Analysis of splitters for self-collimated beams in planar photonic crystals. *Opt. Express* **12**, 1823–1831 (2004).
6. Shi, S. Y., Sharkawy, A., Chen, C. H., Pustai, D. M. & Prather, D. W. Dispersion-based beam splitter in photonic crystals. *Opt. Lett.* **29**, 617–619 (2004).
7. Yu, X. F. & Fan, S. H. Bends and splitters for self-collimated beams in photonic crystals. *Appl. Phys. Lett.* **83**, 3251–3253 (2003).
8. Augustin, M. *et al.* Self-guiding of infrared and visible light in photonic crystal slabs. *Appl. Phys. B* **81**, 313–319 (2005).
9. Yamashita, T. & Summers, C. J. Evaluation of self-collimated beams in photonic crystals for optical interconnect. *IEEE J. Sel. Areas Commun.* **23**, 1341–1347 (2005).
10. Tandon, S. N., Soljacic, M., Petrich, G. S., Joannopoulos, J. D. & Kolodziejski, L. A. The superprism effect using large area 2D-periodic photonic crystal slabs. *Photon. Nanostruct.* **3**, 10–18 (2005).
11. Johnson, S. G. & Joannopoulos, J. D. Block-iterative frequency-domain methods for Maxwell's equations in a planewave basis. *Opt. Express* **8**, 173–190 (2001).
12. Witzens, J., Loncar, M. & Scherer, A. Self-collimation in planar photonic crystals. *IEEE J. Sel. Top. Quantum Electron.* **8**, 1246–1257 (2002).
13. Bourzeix, S. *et al.* Near-field optical imaging of light propagation in semiconductor waveguide structures. *Appl. Phys. Lett.* **73**, 1035–1037 (1998).

Acknowledgements

This work was supported in part by the Materials Research Science and Engineering Center Program of the National Science Foundation, in the Interconnect Focus Center Research Program at the Massachusetts Institute of Technology by the Microelectronics Advanced Research Corporation (MARCO), its participating companies, DARPA, Department of Defence (ONR) MURI and by AFOSR. We gratefully acknowledge Sensors Unlimited for the donation of an infrared camera. M.S.D. is supported by the Portuguese Science and Technology Foundation (FCT). Correspondence and requests for materials should be addressed to P.T.R.

Competing financial interests

The authors declare that they have no competing financial interests.

Reprints and permission information is available online at <http://npg.nature.com/reprintsandpermissions/>